J. Cent. South Univ. (2015) 22: 806−814
DOI: 10.1007/s11771-015-2586-7

Springer

Corrosion behavior of 907 steel under thin electrolyte layers of artificial seawater

WANG Hui-ping(王慧萍)[1], DING Shao-chun(丁少春)[2], ZHU Juan(朱娟)[1],
ZHANG Zhao(张昭)[1], ZHANG Jian-qing(张鉴清)[1, 3], CAO Chu-nan(曹楚南)[1]

1. Department of Chemistry, Zhejiang University, Hangzhou 310027, China;
2. Scientific Research Office, Naval University of Engineering, Wuhan 430033, China;
3. State Key Laboratory for Corrosion and Protection of Metals, Shenyang 110016, China

Abstract: The corrosion behavior of 907 steel under thin electrolyte layer (TEL) has been investigated by means of cathodic polarization curve measurement, electrochemical impedance spectroscopy (EIS) and scanning electron microscopy (SEM). The results show that the cathodic diffusion current density presents the variation trend of initial increase and subsequent decrease with the decrease of TEL thickness, and the maximum deposits at 58 μm. The cotangent-hyperbolic impedance (O) is rationally first introduced to study the diffusion process of the reactants through the corrosion products layer with many permeable holes. The initial corrosion rate of 907 steel under different TEL thickness increases with the decrease of TEL thickness except that of 104 μm, whereas the corrosion rate after long time corrosion can be ranked as 104 μm > 402 μm > 198 μm > 301 μm > bulk solution.

Key words: 907 steel; atmospheric corrosion; electrochemical impedance spectroscopy; polarization

1 Introduction

Atmospheric corrosion (AC) occurs on the metal surface under thin electrolyte layers (TEL) or even adsorbed films [1−4], which has been widely accepted as an electrochemical process in nature, and has been investigated by field exposed tests [5−6], simulated corrosion tests in lab [1−2], electrochemical tests [3−4] and so on. In the early studies on AC processes [7−8], electrochemical method was applied. However, the application of the electrochemical measurement is limited mostly because of the errors caused by the ohmic drop between the reference and working electrodes and the uneven current distribution on the working electrode. To solve these problems, Kelvin probe was adopted in the studies of AC processes by STRATMANN et al [9−11]. But the Volta potential measured by the Kelvin probe was not entirely identical to the corrosion potential under all conditions and the oscillations required by the Kelvin probe measurement can cause significant convective effect in the thin electrolyte layers on the substrate, accelerating the transport of O_2 across the thin electrolyte film [12]. Thus, the conventional electrochemical methods have regained their interest to probe into the AC processes.

The thickness of the TEL plays an important role in the AC process. A change of the TEL thickness affects numbers of corrosion steps, such as the mass transport of the dissolved oxygen and the accumulation of the corrosion products. The former controls the cathodic reaction rate of AC process in a neutral or an alkaline solution, while the later affects the rate of the anodic process [13]. As reported by FRANKEL et al [14], TEL thickness is closely related to the limiting current density associated with oxygen reduction for 304L stainless steel. In our previous work [15−17], the oxygen reduction current is inversely proportional to the layer thickness for copper and aluminum alloys 2024-T3 (in the range of 200−100 μm), while the cathodic reduction is inhibited by the decrease of TEL thickness for AM60 magnesium alloys. In other studies [18−20], the researchers also mentioned the importance of TEL thickness for AC corrosion of many metals or alloys.

It is acknowledged that steel is widely applied as the fundamental material of architectures, vehicles, machineries and so on. Unfortunately, as a great variety of structures and metallic equipments are exposed to the atmosphere, the steel corrosion is very serious which accounts for half of the total corrosion loss. Therefore,

Foundation item: Projects(21073162, 21273199) supported by the National Natural Science Foundation of China; Project(GCTKF2012013) supported by the Science and Technology Bureau of Jiaxing Municipality and the State Key Laboratory Breeding Base of Green Chemistry-Synthesis Technology, China
Received date: 2013−12−09; **Accepted date:** 2014−03−15
Corresponding author: ZHANG Zhao, Professor, PhD; Tel: +86−571−85615190; E-mail: eaglezzy@zjuem.zju.edu.cn

the study of the steel corrosion in atmosphere has been popular for decades. Much field exposed tests have been performed to investigate the AC corrosion of different steels in different exposure environments. Among these studies, chloride ion and SO_2 are investigated as the main influencing factors because chloride ion is an important natural contaminant to enhance metal corrosion, while SO_2 is an extremely industrial corrosive gas due to its high solubility in water and acidization effect [21]. SINGH et al [22] found that the presence of SO_2 and salinity in the environment changed the structure and protective properties of the rusts formed on the steel surface. According to MA et al [23], chloride ion influences the corrosion rate, the morphology and the composition of the rust layer as well. AC corrosion of carbon steel in different marine sites tested by CASTAÑO et al [24] and SYED [25] indicated that the major constituents of the rusts were lepidocrocite and goethite when chloride ion and SO_2 were taken into account as the contaminants. A new study by WANG et al [26] showed that the influence of environment conditions is greater compared to the steel composition.

To acquire the details of the steel corrosion behavior within a short time, the simulated corrosion test in lab is widely applied [27−32]. Compared with the real marine atmospheric environment, electrolyte comprising chloride or/and sulphate ions in these researches is too simple. Consequently, these tests cannot simulate the real AC corrosion of steels accurately. In the present work, artificial seawater, which is more representative of the marine environment, is applied to solve this problem.

The 907 steel is a kind of typical marine materials, which is widely used as the components of many watercrafts, and suffers from severe AC corrosion during its long-term exposure in marine atmosphere. However, according to our knowledge, there is less literature reporting the AC corrosion behavior of 907 steel. The goal of this work is to gain some insight into the AC corrosion behavior of 907 steel using cathodic polarization curves, EIS and SEM techniques.

2 Experimental

2.1 Materials

The artificial seawater was prepared from analytical grade reagent and double-distilled water. The basic composition of this electrolyte is given in Table 1. And the pH is found to be about 7.0.

Table 1 Chemical compositions of artificial seawater used (mg/L)

Cl^-	Br^-	CO_3^{2-}	SO_4^{2-}	Na^+	K^+	Mg^{2+}	Ca^{2+}
20237.2	72.9	1066.3	3237.2	11131.5	423	1366.6	650.4

The 907 steel embedded in nylon holder with an exposing area of 0.126 cm^2 was used as the working electrode. A circle type Pt wire (0.3 mm in diameter) and a saturated calomel electrode (SCE) served as the counter electrode and the reference electrode, respectively. Prior to each experiment, the working surface was polished with different grits of emery paper and alumina powder, then thoroughly rinsed with double-distilled water, degreased with acetone, and dried in cool flowing air.

2.2 TEL set-up

The experimental arrangement used in this work is the same as reported in our previous study [15], except that the SCE is not inserted in the bulk solution directly but through a salt bridge (KCl) to reduce the permeation of KCl from SCE to the bulk solution.

2.3 Electrochemical measurements

Electrochemical measurements including cathodic polarization curves and electrochemical impedance spectroscopy (EIS) were conducted using an electrochemical measurement unit (PARSTAT 2273, Advanced Electrochemical System), and all the potentials not otherwise specified in this work were referred to SCE. As described in Refs. [15, 21, 29], anodic polarization curves under TEL were greatly influenced by the uneven distribution of the current density which was concentrated on the brim of the electrodes. Nevertheless, in the case of cathodic polarization, the cathodic current was mainly caused by the reduction of oxygen and/or corrosion products, and the current density distributed more uniformly on the whole electrode surface [33]. Therefore, only cathodic polarization was carried out in this work. The cathodic polarization curves were performed from the open circuit potential (OCP) to −1.4 V with a sweep rate of 0.5 mV/s after immersion for 30 min. EIS tests were conducted over the frequency range from 100 kHz to 10 mHz at the OCP with a sinusoidal potential perturbation of 5 mV. ZSimpWin software was used to analyze the EIS data. For better reproducibility, the electrochemical measurements were repeated at least two times. And all electrochemical measurements were carried out at 15 ºC.

2.4 SEM

After corrosion, the working electrode surface was rinsed with double-distilled water, dried in cool flowing air, and then characterized using scanning electron microscope (SEM, Hitachi SU70). Before SEM observation, the surface of specimen was sputtered with gold powder.

3 Results and discussion

3.1 Cathodic polarization curves

Figure 1 presents the cathodic polarization plots of 907 steel under different TEL thickness. It is apparent that these curves can be divided into three segments: Region I in the vicinity of the OCP represents the weak polarization, Region II characterizes the diffusion-controlled process where both oxygen and corrosion products can be reduced at more negative potentials [21, 33], and Region III mainly corresponds to the hydrogen evolution reaction.

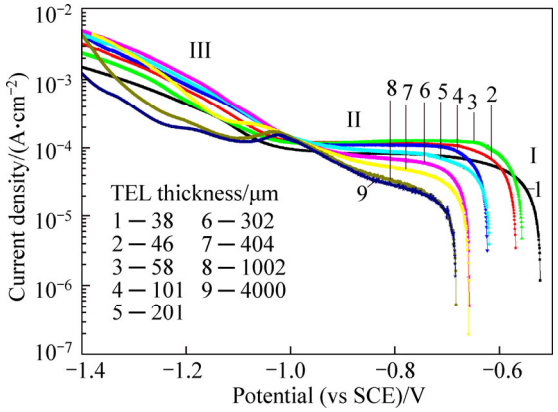

Fig. 1 Cathodic polarization curves of 907 steel under TEL with different thickness

In Region II, there exists a current platform for the TEL thickness of 46, 58 and 101 μm, which indicates that the cathodic reactions for the TEL thickness are completely diffusion-controlled. While the current density increases with potential for other TEL thickness, which indicates that the cathodic reactions for these TEL thickness are mainly diffusion-controlled, and potential dependent somewhat. The influencing extent of the potential on the current density increases from 201 μm, through 302, 404, 1002 and finally to 4000 μm (Fig. 1). When comparing the current densities under different TEL thickness in Region II, it can be seen that the current density under different TEL thickness is larger than that in bulk solution (>1000 μm).

The current densities taken at the midpoint potential of each straight line in Region II (Fig. 1) are adopted to present the relationship of the thickness and current density (Fig. 2) intuitively. From Fig. 2, it can be clearly seen that the current density shows the variation trend of initial increase and subsequent decrease with the increase of TEL thickness, and the maximum value deposits at 58 μm.

The overall current measured in Fig. 1 mainly originates from the cathodic current of the electrode because in the cathodic polarization process, the anodic reactions (including the metal dissolution and the

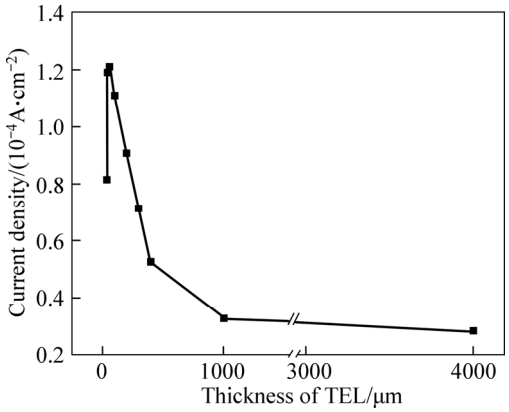

Fig. 2 Cathodic polarization current densities taken at midpoint potential of each straight lines in Region II

diffusion of metal ions) are inhibited, and therefore the anodic current can be negligible. When the cathodic diffusion process is mainly considered, the cathodic current for the corroded electrode can be expressed by the following equation [15−16, 34]:

$$J_c = \frac{J_{corr}\exp\left(-\frac{\Delta E}{\beta_c}\right)}{1-\frac{J_{corr}}{J_{lim}}\left[1-\exp\left(-\frac{\Delta E}{\beta_c}\right)\right]} \quad (1)$$

where J_c is the cathodic current density, J_{corr} is the corrosion current density at OCP, ΔE is the overpotential, β_c is the cathodic Tafel slope, and J_{lim} is the diffusion limiting current density. It can be seen that J_c is determined by J_{lim} if other parameters are constant, and the greater the value of J_{lim}, the larger the value of J_c.

The theoretical J_{lim} for the one-dimensional diffusion can be calculated according to the Nernst-Fick equation [15−16, 34]:

$$J_{lim} = nFD_{O_2}[O_2]/\delta \quad (2)$$

where D_{O_2} and $[O_2]$ are the diffusion coefficient and the concentration of the dissolved oxygen in the electrolyte, respectively, n is the number of the electrons involved in the oxygen reduction reaction, F is the Faraday constant, and δ is the thickness of the diffusion layer. As reported in Ref. [35], δ is in the range of 10^{-4}–10^{-5} m. According to Eq. (2), J_{lim} is determined by δ, and the smaller the δ, the greater the J_{lim}.

For thick electrolyte layer (from 1002 to 4000 μm), it consists of two parts: a diffusion layer (inner layer) and a convection layer. In this case, the change of the TEL thickness affects mainly the convection layer and δ can be regarded as a constant. Therefore, according to Eq. (2) and when considering that both D_{O_2} in diffusion layer and $[O_2]$ in convection layer are constant, J_{lim} can also be regarded as a constant, which makes TEL thickness have negligible influence on the cathodic limiting current

density (Fig. 2).

In the thickness range of 58−1002 μm, especially from 58 to 404 μm, J_{lim} increases rapidly with the decrease of the TEL thickness, implying that the TEL thickness is in the range of diffusion layer and the cathodic reactions are mainly diffusion-controlled. The thinning of the electrolyte layer means the decrease of δ and thus the increase of the diffusion limiting current density. With further thinning of the layer thickness and when the thickness is less than 58 μm, the current density decreases sharply. Two reasons might be responsible for this phenomenon. As a consequence of the O_2 reduction, high alkaline conditions will prevail in the thin electrolyte and therefore allow the surface to be passivated easily. In addition, the metal ions generated by the dissolution will precipitate immediately at the interface metal/electrolyte because the limit of its solubility is reached. As the consequence of the precipitation, large parts of the surface are blocked and the anodic metal dissolution is retarded [10].

As previously reported in Refs. [21, 33], in the oxygen diffusion controlling range, both oxygen and corrosion products can be reduced. Obviously in Fig. 1, there is a current peak in the vicinity of −1.05 V when the electrolyte layer is thick. This may be ascribed to the reduction of O_2 and the corrosion products formed during the stabilization of the OCP.

3.2 EIS measurements

The Nyquist diagrams and Bode plots for 907 steel under different TEL thickness during different immersion time are shown in Figs. 3 and 4, respectively.

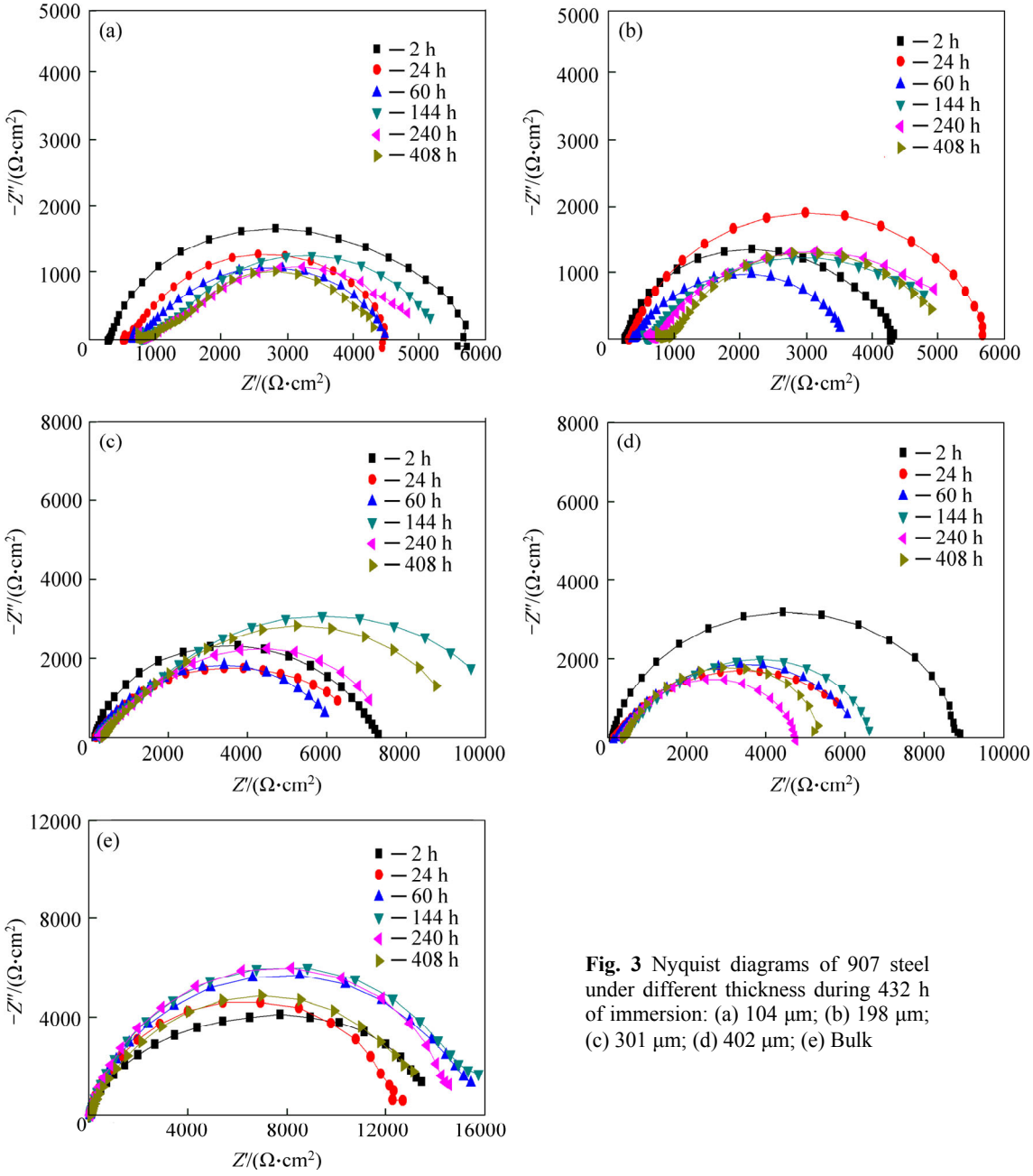

Fig. 3 Nyquist diagrams of 907 steel under different thickness during 432 h of immersion: (a) 104 μm; (b) 198 μm; (c) 301 μm; (d) 402 μm; (e) Bulk

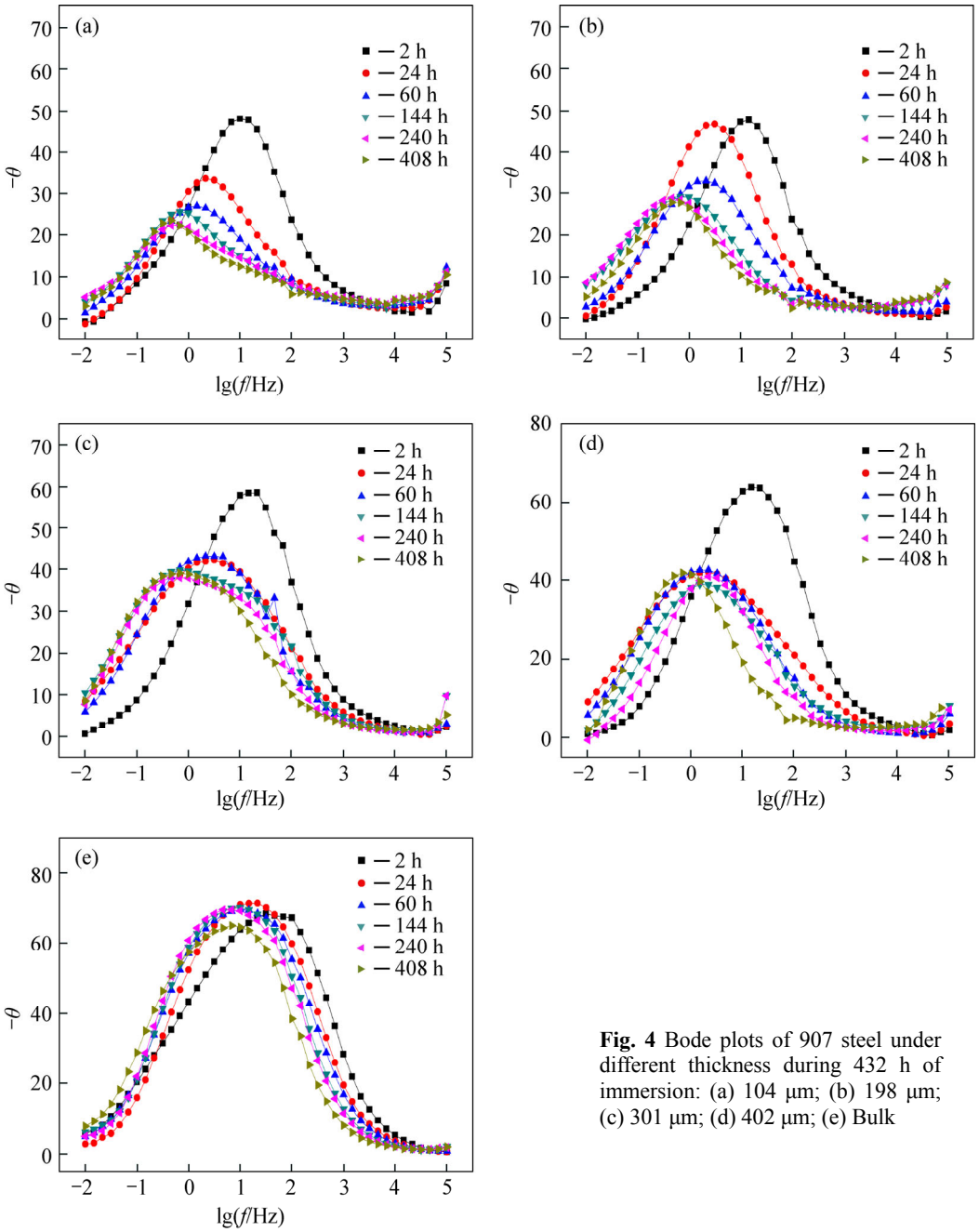

Fig. 4 Bode plots of 907 steel under different thickness during 432 h of immersion: (a) 104 μm; (b) 198 μm; (c) 301 μm; (d) 402 μm; (e) Bulk

The time-constant numbers of EIS plots have been determined through both the features of the EIS diagrams (such as the number of the phase angle peak in Bode plot, the number of the slopes in Bode plot and the number of the capacitance in Nyquist plot), and the method developed by CAMPESTRINI et al [36] simultaneously. The analyzed results show that, each of the EIS plots contains two time constants corresponding to two capacitive arcs at high and intermediate frequencies, respectively. Due to the overlap of the two capacitive arcs, the two time constants are not identified easily.

Two different electrochemical equivalent circuit (EEC) models are proposed, as shown in Fig. 5, in which R_s is the solution resistance, R_f is the film resistance and CPE1 is the film capacitance, R_{ct} and CPE2 represent the charge transfer resistance and double-layer capacitance, respectively, and "O" is the cotangent-hyperbolic diffusion impedance introduced to study the diffusion process of the reactants through permeable defects (e.g. pores) [37]. In the Nyquist diagrams, part of the capacitive loop appears in the high-frequency with the proceeding of the corrosion, which may be caused by the relaxation process of the solution resistance and capacitance in the etch pit [38].

Figures 6 and 7 show typical Nyquist diagrams and Bode plots for two given TEL thicknesses of 104 μm and 301 μm, respectively. It can be seen that the experimental data and the fitted data match well, inferring that the

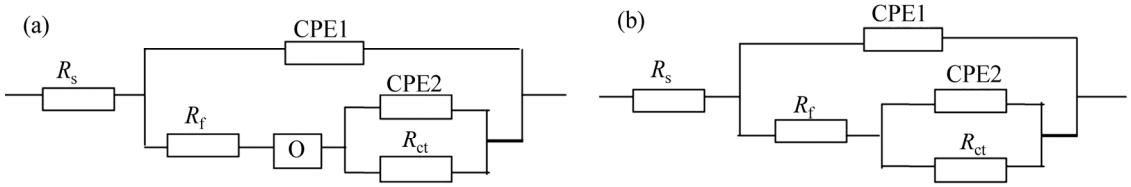

Fig. 5 EEC models proposed for fitting EIS data of 907 steel under different TEL thickness: (a) 104 μm (after 60 h); (b) Other cases

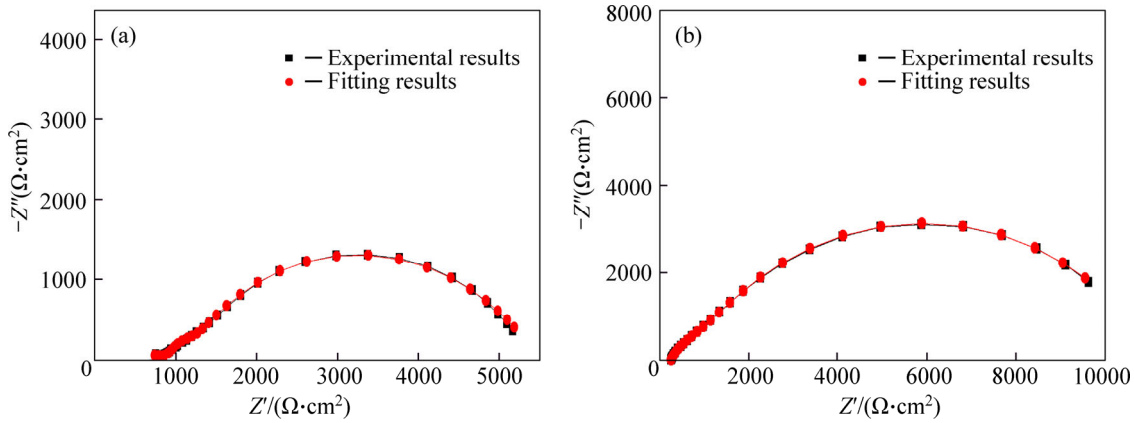

Fig. 6 Nyquist diagrams of 907 steel under two given TEL thickness at immersion time of 144 h: (a) 104 μm; (b) 301μm

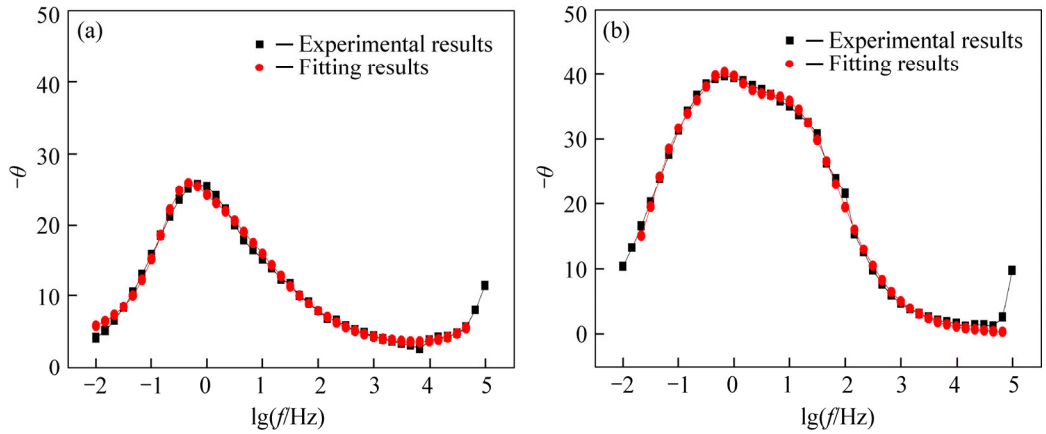

Fig. 7 Bode plots of 907 steel under two given TEL thickness at immersion time of 144 h: (a) 104 μm; (b) 301μm

applied equivalent circuits are reliable. Then, there exists a problem: why the cotangent- hyperbolic diffusion impedance (O) in Fig. 5(a) (for 104 μm) should be introduced? In order to elucidate this question, the surface morphologies of some typical corroding electrodes after long time corrosion (432 h) are analyzed using SEM technique (Fig. 8). It can be seen that, in the case of 104 μm, the corrosion product layer possesses numerous holes of different sizes and shapes (Fig. 8(a)) and may act as the porous coatings [37]. The holes provide plentiful tunnels for corrosive species such as chloride ions to penetrate into the substrate, which results in the presence of the cotangent-hyperbolic diffusion element (O) in Fig. 5(a).

Generally, the reciprocal of the polarization resistance (R_p) is used to evaluate the corrosion rate [13, 30, 39]. However, erroneous corrosion rate will be resulted when more than one state variable affects EIS apart from potential, and thus, R_{ct} is taken to calculate the corrosion rate because of its close correlation with the corrosion rate [40]. Owing to the overlap of the two time constants at high and low frequency and the mathematics process executed in fitting process, the fitted results of R_f and R_{ct} are not well distinguished. Furthermore, surface film protects steel substrate to some extent. Therefore, the sum of R_f and R_{ct} is applied to characterize corrosion resistance, and the larger the sum value, the less the corrosion rate. The reciprocal of the sum of R_f and R_{ct} as a function of the immersion time is shown in Fig. 9. It can be seen that the corrosion rate of 907 steel under different TEL thickness is always higher than that in the bulk solution, which agrees well with the results obtained from polarization tests.

In the first 2 h of immersion (Fig. 10), all corrosion

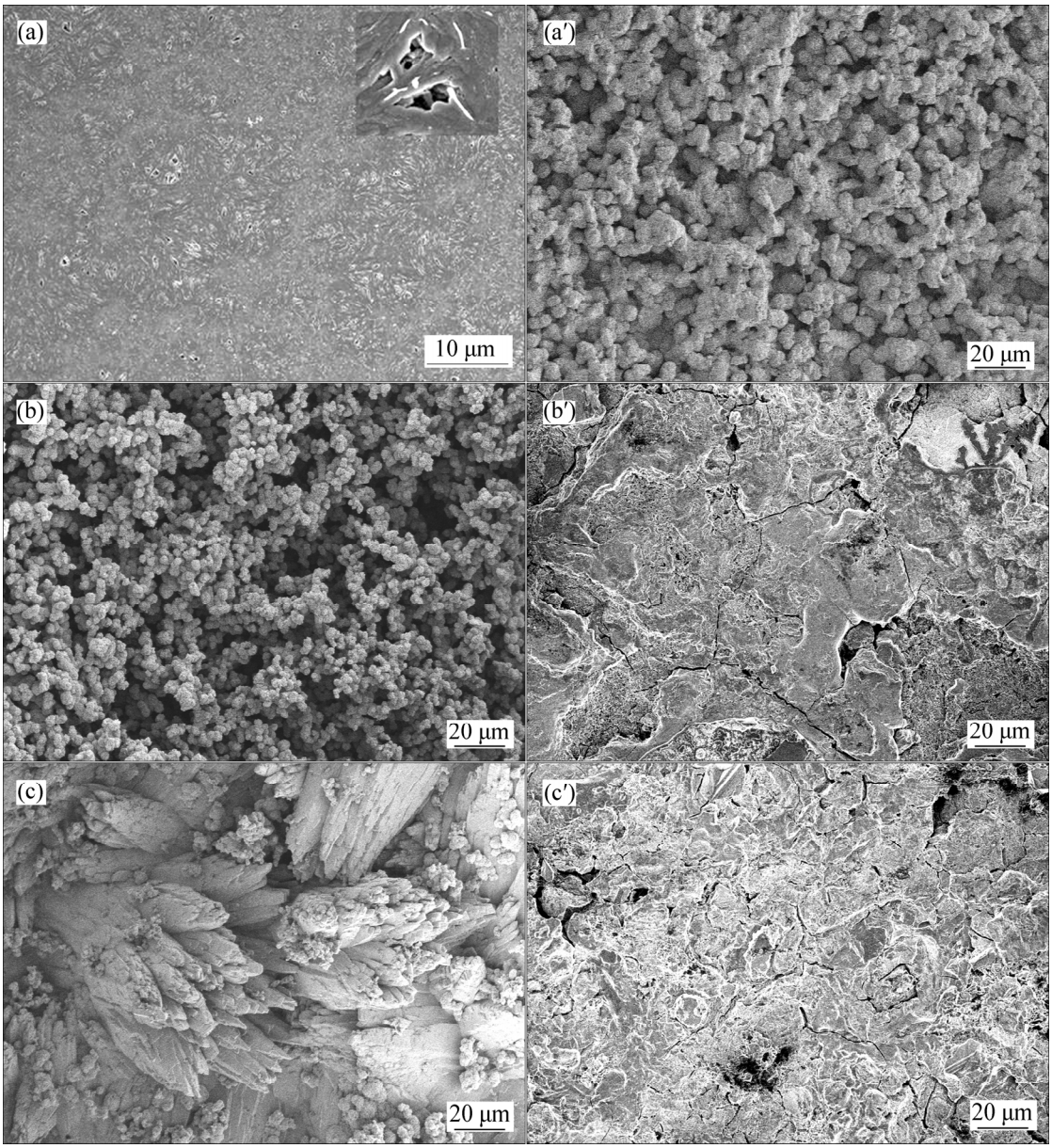

Fig. 8 SEM micrographs of outer rust layer (a−c) and inner rust layer (a′−c′) after 432 h immersion: (a, a′) 104 μm; (b, b′) 301 μm; (c, c′) Bulk solution

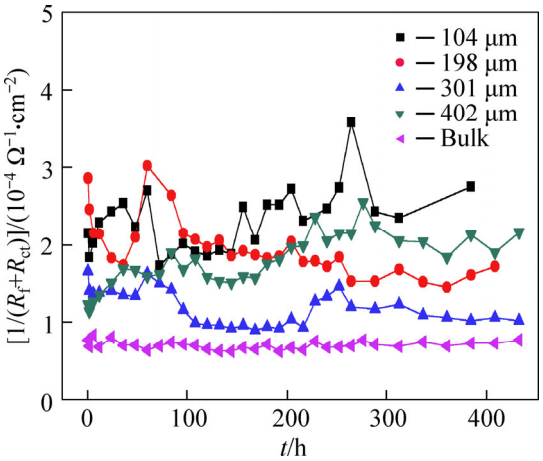

Fig. 9 Variation of corrosion rates for 907 steel with immersion time (0−480 h) under different electrolyte layer thickness

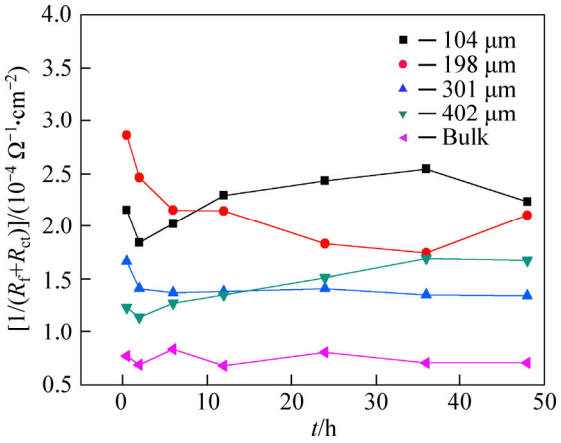

Fig. 10 Variation of corrosion rates for 907 steel with immersion time (0−48 h) under different electrolyte layer thickness

rates decrease, which may be originated from the formation of corrosion products such as iron hydroxyl compounds. By comparing the corrosion rates at the same immersion time under different TEL thickness in the first 5 h, the corrosion rate increases with the decrease of TEL thickness except the abnormality of 104 μm, which is different from the polarization results, probably due to the large cathodic overpotential forced on the electrode by the latter technique. On the other hand, the above difference between EIS and polarization results may also be attributed to the facts that the cathodic reactions for the TEL thickness of 104 μm are completely diffusion-controlled (Fig. 1), while those for other TEL thickness are somewhat potential-dependent as elucidated above.

After long immersion time (>216 h), the corrosion rate can be ranked as 104 μm > 402 μm>198 μm > 301 μm > bulk solution, which differs from the corrosion regulation in the initial short time (Fig. 9). This phenomenon may be resulted from many factors, such as the change of the O_2 transfer rate, the different structures of the corrosion product layers (including the outer and the inner rust layer) formed on the electrode surface after long time immersion, the accumulation and peeling off of the corrosion product layer.

4 Conclusions

1) The cathodic diffusion current density of 907 steel under different TEL thickness increases with the decrease of TEL thickness until 58 μm due to the easier transfer of oxygen through the electrolyte layer. With further reduction of TEL thickness from 58 μm to 38 μm, the diffusion current density decreases probably due to the passivation of the substrate surface caused by O_2 reduction.

2) The cotangent-hyperbolic impedance (O) is rationally first introduced to fit the EIS data of 104 μm because of the existence of corrosion product layer with many permeable holes. The initial corrosion rate of 907 steel under different TEL thickness increases with the decrease of TEL thickness except that of 104 μm. After long time corrosion, the order of the corrosion rate changes as 104 μm > 402 μm > 198 μm > 301 μm > bulk solution.

References

[1] KATAYAMA H. NODA K, MASUDA H, NAGASAWA M, ITAGAKI M, WATANABE K. Corrosion simulation of carbon steels in atmospheric environment [J]. Corrosion Science, 2005, 47(10): 2599−2606.

[2] HAN Wei, YU Guo-cai, WANG Zhen-yao, WANG Jun. Characterisation of initial atmospheric corrosion carbon steels by field exposure and laboratory simulation [J]. Corrosion Science, 2007, 49(7): 2920−2935.

[3] ABREU C M, CRISTÓBAL M J, NÓVOA X R, PENA G, PÉREZ M C. Electrochemical behaviour of an AISI 304L stainless steel implanted with nitrogen [J]. Electrochimica Acta, 2008, 53(20): 6000−6007.

[4] XU Jian, WU Xin-qiang, HAN E-H. The evolution of electrochemical behaviour and oxide film properties of 304 stainless steel in high temperature aqueous environment [J]. Electrochimica Acta, 2012, 71: 219−226.

[5] OH S J, COOK D C, TOWNSEND H E. Atmospheric corrosion of different steels in marine, rural and industrial environments [J]. Corrosion Science, 1999, 41(9): 1687−1702.

[6] HOU W, LIANG C. Eight-year atmospheric corrosion exposure of steels in China [J]. Corrosion, 1999, 55(1): 65−73.

[7] MANSFELD F, TSAI S. Laboratory studies of atmospheric corrosion−I. Weight loss and electrochemical measurements [J]. Corrosion Science, 1980, 20(7): 853−872.

[8] MANSFELD F. Atmospheric corrosion rates, time-of-wetness and relative humidity [J]. Materials and Corrosion, 1979, 30(1): 38−42.

[9] STRATMANN M, STRECKEL H. On the atmospheric corrosion of metals which are covered with thin electrolyte layers−I. Verification of the experimental technique [J]. Corrosion Science, 1990, 30(6/7): 681−696.

[10] STRATMANN M, STRECKEL H. On the atmospheric corrosion of metals which are covered with thin electrolyte layers−II. Experimental results [J]. Corrosion Science, 1990, 30(6/7): 697−714.

[11] STRATMANN M, STRECKEL H, KIM K T, CROCKETT S. On the atmospheric corrosion of metals which are covered with thin electrolyte layers−III. The measurement of polarisation curves on metal surfaces which are covered by thin electrolyte layers [J]. Corrosion Science, 1990, 30(6/7): 715−734.

[12] COX A, LYON S B. An electrochemical study of the atmospheric corrosion of mild steel−I. Experimental method [J]. Corrosion Science, 1994, 36(7): 1167−1176.

[13] NISHIKATA A, ICHIHARA Y, TSURU T. An application of electrochemical impedance spectroscopy to atmospheric corrosion study [J]. Corrosion Science, 1995, 37(6): 897−911.

[14] FRANKEL G S, STRATMANN M, ROHWERDER M, MICHALIK A, MAIER B, DORA J, WICINSKI M. Potential control under thin aqueous layers using a Kelvin Probe [J]. Corrosion Science, 2007, 49(4): 2021−2036.

[15] CHENG Ying-liang, ZHANG Zhao, CAO Fa-he, LI Jin-feng, ZHANG Jian-qing, WANG Jian-min, CAO Chu-nan. A study of the corrosion of aluminum alloy 2024-T3 under thin electrolyte layers [J]. Corrosion Science, 2004, 46(7): 1649−1667.

[16] LIU Wen-juan, CAO Fa-he, CHEN An-na, CHANG Lin-rong, ZHANG Jian-qing, CAO Chu-nan. Corrosion behaviour of AM60 magnesium alloys containing Ce or La under thin electrolyte layers. Part 1: Microstructural characterization and electrochemical behaviour [J]. Corrosion Science, 2010, 52(2): 627−638.

[17] LIAO Xiao-ning, CAO Fa-he, ZHENG Li-yun, LIU Wen-juan, CHEN An-na, ZHANG Jian-qing, CAO Chu-nan. Corrosion behaviour of copper under chloride-containing thin electrolyte layer [J]. Corrosion Science, 2011, 53(10): 3289−3298.

[18] ZHANG Tao, CHEN Chong-mu, SHAO Ya-wei, MENG Guo-zhe, WANG Fu-hui, LI Xiao-gang, DONG Chao-fang. Corrosion of pure magnesium under thin electrolyte layers [J]. Electrochimica Acta, 2008, 53(27): 7921−7931.

[19] ZHOU H R, LI X G, MA J, DONG C F, HUANG Y Z. Dependence of the corrosion behavior of aluminum alloy 7075 on the thin electrolyte layers [J]. Materials Science and Engineering B, 2009, 162(1): 1−8.

[20] ZHENG Li-yun, CAO Fa-he, LIU Wen-juan, JIA Bing-li, ZHANG

Jian-qing. Corrosion behavior of Pure zinc and its alloy under thin electrolyte layer [J]. Acta Metallurgica Sinica (English Letters), 2010, 23(6): 416−430.

[21] HUANG Hua-liang, DONG Ze-hua, CHEN Zhen-yu, GUO Xing-peng. The effects of Cl^- ion concentration and relative humidity on atmospheric corrosion behaviour of PCB-Cu under adsorbed thin electrolyte layer [J]. Corrosion Science, 2011, 53(4): 1230−1236.

[22] SINGH D D N, YADAV S, SAHA J K. Role of climatic conditions on corrosion characteristics of structural steels [J]. Corrosion Science, 2008, 50(1): 93−110.

[23] MA Yuan-tai, LI Ying, WANG Fu-hui. Corrosion of low carbon steel in atmospheric environments of different chloride content [J]. Corrosion Science, 2009, 51(5): 997−1006.

[24] CASTAÑO J G, BOTERO C A, RESTREPO A H, AGUDELO E A, CORREA E, ECHEVERRÍA F. Atmospheric corrosion of carbon steel in Colombia [J]. Corrosion Science, 2010, 52(1): 216−223.

[25] SYED S. Atmospheric corrosion of carbon steel at marine sites in saudi arabia [J]. Materials and Corrosion, 2010, 61(3): 238−244.

[26] WANG Zhi-feng, LIU Jian-rong, WU Li-xin, HAN Rong-dong, SUN Yi-qiang. Study of the corrosion behavior of weathering steels in atmospheric environments [J]. Corrosion Science, 2013, 67: 1−10.

[27] CRUZ R P V, NISHIKATA A, TSURU T. AC impedance monitoring of pitting corrosion of stainless steel under a wet-dry cyclic condition in chloride-dontaining environment [J]. Corrosion Science, 1996, 38(8): 1397−1406.

[28] NISHIKATA A, YAMASHITA Y, KATAYAMA H, TSURU T, USAMI A, TANABE K, MABUCHI H. An electrochemical impedance study on atmospheric corrosion of steels in a cyclic wet-dry condition [J]. Corrosion Science, 1995, 37(12): 2059−2069.

[29] NISHIKATA A, ICHIHARA Y, TSURU T. Electrochemical impedance spectroscopy of metals covered with a thin electrolyte layer [J]. Electrochimica Acta, 1996, 41(7/8): 1057−1062.

[30] NISHIKATA A, ICHIHARA Y, HAYASHI Y, TSURU T. Influence of electrolyte layer thickness and pH on the initial stage of the atmospheric corrosion of iron [J]. Journal of the Electrochemical Society, 1997, 144(4): 1244−1252.

[31] CHUNG K-W, KIM K-B. A study of the effect of concentration build-up of electrolyte on the atmosphericcorrosion of carbonsteel during drying [J]. Corrosion Science, 2000, 42(3): 517−531.

[32] DUBUISSON E, LAVIE P, DALARD F, CAIRE J-P, SZUNERITS S. Study of the atmospheric corrosion of galvanised steel in a micrometric electrolytic droplet [J]. Electrochemistry Communications, 2006, 8(6): 911−915.

[33] HUANG Hua-liang, GUO Xing-peng, ZHANG Guo-an, DONG Ze-hua. The effects of temperature and electric field on atmospheric corrosion behaviour of PCB-Cu under absorbed thin electrolyte layer [J]. Corrosion Science, 2011, 53(5): 1700−1707.

[34] CAO Chu-nan. Estimation of electrochemical kinetic parameters of corrosion processes by weak polarization curve fitting [J]. Journal of Chinese Society for Corrosion and Protection, 1985, 5(3): 155−164.

[35] GUO He-tong, TAN Qi-xian. study of the electrochemistry [M]. Tianjin: Tianjin University Press, 2000: 225. (in Chinese)

[36] CAMPESTRINI P, WESTING E P M, WIT J H W. Influence of surface preparation on performance of chromate conversion coatings on Alclad 2024 aluminium alloy. Part II: EIS investigation [J]. Electrochimica Acta, 2001, 46(17): 2631−2647.

[37] LIU C, BI Q, LEYLAND A, MATTHEWS A. An electrochemical impedance spectroscopy study of the corrosion behaviour of PVD coated steels in 0.5 N NaCl aqueous solution. Part II: EIS interpretation of corrosion behaviour [J]. Corrosion Science, 2003, 45(6): 1257−1273.

[38] SHAO Hai-bo. Electrochemical behavior and inhibitors of aluminum in alkaline solutions [D]. Hangzhou: Zhejiang University, 2004. (in Chinese)

[39] EI-MAHDY G A, NISHIKATA A, TSURU T. AC impedance study on corrosion of 55%Al-Zn alloy-coated steel under thin electrolyte layers [J]. Corrosion Science, 2000, 42(9): 1509−1521.

[40] LORENZ W J, MANSFELD F. Determination of corrosion rates by electrochemical DC and AC methods [J]. Corrosion Science, 1981, 21(9/10): 647−672.

(Edited by YANG Bing)